



Deposited via The University of York.

White Rose Research Online URL for this paper:

<https://eprints.whiterose.ac.uk/id/eprint/198850/>

Version: Accepted Version

---

**Article:**

Pfukwa, Ngaatendwe B. C., Rautenbach, Marina, Hunt, Neil Terrence et al. (2023) Temperature induced effects on the structure of Gramicidin S. *Journal of Physical Chemistry B*. 3774–3786. ISSN: 1520-5207

<https://doi.org/10.1021/acs.jpcb.2c06115>

---

**Reuse**

Items deposited in White Rose Research Online are protected by copyright, with all rights reserved unless indicated otherwise. They may be downloaded and/or printed for private study, or other acts as permitted by national copyright laws. The publisher or other rights holders may allow further reproduction and re-use of the full text version. This is indicated by the licence information on the White Rose Research Online record for the item.

**Takedown**

If you consider content in White Rose Research Online to be in breach of UK law, please notify us by emailing [eprints@whiterose.ac.uk](mailto:eprints@whiterose.ac.uk) including the URL of the record and the reason for the withdrawal request.

# Temperature induced effects on the structure of Gramicidin S

Ngaatendwe B. C. Pfukwa,<sup>a</sup> Marina Rautenbach,<sup>b</sup> Neil T. Hunt,<sup>c,d</sup> Olufemi O. Olaoye,<sup>a</sup> Vikas Kumar,<sup>b</sup> Anthony W. Parker<sup>a,e</sup> Lucy Minnes,<sup>c</sup> and Pieter H. Neethling<sup>a,\*</sup>

<sup>a</sup> Department of Physics, Laser Research Institute, Stellenbosch University, Private Bag X1, Matieland, 7602, South Africa

<sup>b</sup> BIOPEP Peptide Group, Department of Biochemistry, Stellenbosch University, Private Bag X1, Matieland, 7602, South Africa

<sup>c</sup> Department of Physics, University of Strathclyde, SUPA, 107 Rottenrow East, Glasgow, G4 0NG, United Kingdom

<sup>d</sup> Department of Chemistry and York Biomedical Research Institute, University of York, Heslington, York, YO10 5DD, United Kingdom

<sup>e</sup> STFC Central Laser Facility, Research Complex at Harwell, Rutherford Appleton Laboratory, Harwell Science and Innovation Campus, Didcot, Oxon, OX11 0QX, United Kingdom

\*Email: pietern@sun.ac.za

**ABSTRACT:** We report on the structure of Gramicidin S (GS) in a model membrane mimetic environment represented by the amphipathic solvent 1-octanol using 1D and 2D IR spectroscopy. To explore potential structural changes of GS we also performed a series of spectroscopic measurements at differing temperatures. By analysing the amide I band and using 2D-IR spectral changes results could be associated to disruption of aggregates/oligomers, as well as structural and conformational changes happening in concentrated solution of GS. The ability of 2D-IR to enable differentiation in melting transitions of oligomerised GS structures is attributed to the sensitivity of the technique to vibrational coupling. Two melting transition temperatures were identified; at  $T_{m1}$  in the range 41 – 47 °C where the GS aggregates disassemble and at  $T_{m2} = 57 \pm 2$  °C where there is significant change involving GS  $\beta$ -sheet-type hydrogen-bonds whereby there is proposed to be loss of interpeptide hydrogen-bonds of smaller oligomers. Further analysis with QM/MM simulations and 2<sup>nd</sup> derivative results highlighted participation of active GS side chains. Ultimately, this work contributes towards understanding GS structure and the formulation of GS analogues with improved bioactivity.

## 1. INTRODUCTION

Gramicidin S (GS) [*cyclo*-(L-Val–L-Orn–L-Leu–D-Phe–L-Pro)<sub>2</sub>] is an amphipathic cyclic cationic decapeptide produced by *Aneurinibacillus migulanus*, formerly known as *Bacillus brevis*.<sup>1</sup> The secondary structure of GS has an intrapeptide  $\beta$ -sheet conformation formed by two antiparallel  $\beta$ -strands from the tripeptide sequences (Val-Orn-Leu) interconnected at both ends by two type II'  $\beta$ -turns formed by D-Phe-Pro residues [Figure 1](#). The GS molecule is amphiphilic, with the two charged Orn side chains and the two D-Phe rings projecting from one side of the molecule while the four hydrophobic Val and Leu side chains project from the other side.<sup>2</sup> As an antimicrobial peptide (AMP), the spatial structure of GS is important in its interaction with target cell membranes. The main target of cationic amphiphiles is the bacterial membrane.<sup>3</sup> In its working mechanism, the cationic amino acid residues interact with the outer leaflet of the bacterial membrane, enabled by penetration of the hydrophobic amino acid residues into the lipid bilayer.<sup>3</sup> This action compromises the structural integrity of the phospholipid bilayer, inducing pores or forming channels that consequently disrupt the electrical insulation properties of the lipid membranes.<sup>3,4</sup> There is considerable evidence that GS permeabilises the lipid bilayer of bacterial membranes.<sup>5–7</sup> However, a recent study concluded that mode of action of GS is primarily focused on the bacterial membrane, but also entails other targets such as membrane proteins and DNA packing.<sup>8</sup>

Due to its well-defined structure, GS has been utilised as a model peptide antibiotic possessing high antibacterial activity against a broad range of Gram-negative and Gram-positive bacterial strains.<sup>8,9</sup>

No resistance has been observed for GS towards its clinical use in treating infections, which makes GS an ideal peptide to address the rise in bacterial resistance towards conventional drugs.<sup>10</sup> However, due to its high haemolytic activity it has been limited to topical applications although some efforts have been made towards generating GS analogues with increased antimicrobial activity and lower toxicity.<sup>5,11–13</sup> Given the importance of GS structure in relation to its biological activity we seek to better understand the GS solution structure and relate it to activity, providing information to guide the design of GS analogues with improved selectivity.

The goal of this work is to understand the structure of GS in a model membrane mimetic environment, 1-octanol, using one and two dimensional (1D and 2D) IR spectroscopy. The solvent octanol as an amphipathic alcohol complements the amphipathic nature of GS, in addition to its properties such as high temperature stability, lack of significant spectral interference/overlap with the GS amide I mode and the solubility of GS. Studies have shown that physicochemical properties are important in correlating bioactivity and chemical structure<sup>14</sup>. In early 1960s, Corwin Hansch et al. first determined the octanol/water partition coefficient system (log P) which became a standard system for the description of lipophilicity for reasons; 1) octanol serves as a good mimic for the long hydrocarbon chains with a polar headgroup found in membranes, 2) octanol dissolves water thus, emulating the aqueous component of biological hydrophobic regions such as membranes and 3) octanol is cheap, easy to purify and lacks a chromophore, which would interfere with the spectroscopic determination of compound concentrations<sup>14–19</sup>.

In this study we showed that temperature induced changes in the GS 2D-IR spectra can be correlated to the two steps disruption of aggregates/oligomers in a concentrated solution of GS. Analysis of the amide I band of GS enabled insights into the conformational behaviour of GS in solution alongside identification of structural changes in GS and GS oligomers/aggregates. A conformational change of GS, which possibly involved a hydrogen bonded network, was previously proposed in aqueous solutions and it was observed that an increase in GS concentration and a longer time in solution causes unusual changes in surface tension and spectrophotometric character.<sup>20</sup> Generally, biological temperatures are considered to be in the range 35 – 45 °C where most proteins/peptides are stable. However, to identify the potential of IR/2D-IR to resolve structural changes of GS temperatures used in this study were chosen to maximise disruption. We therefore report the use of temperature to perturb the structure of the peptide sequence and demonstrate the ability of 2D-IR to observe these differences and to show that the structure was disrupted. Furthermore, the information obtained on the GS model cyclodecapeptide system, will assist in the development of *ab initio* predictions of peptide structure, and so facilitate 2D-IR simulations on more complex members of the cyclodecapeptide group, in particular promoting developments of advanced antimicrobial agents.

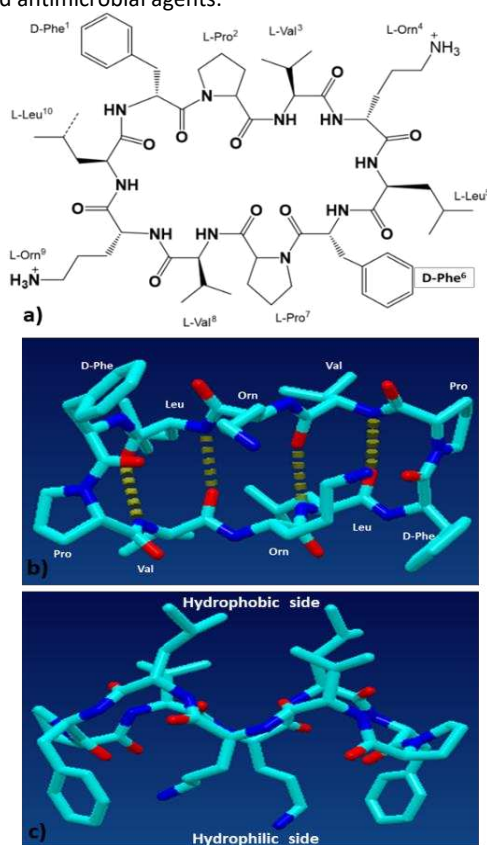


**Figure 1.** Structure of gramicidin S with monoisotopic Mr of 1140.7059. The primary structure of GS is shown in a). Residues are referred to using standard three letter amino acid abbreviations with Orn representing ornithine. Residues are numbered according to their order of incorporation during biological synthesis. A modelled low energy 3D structure of GS is shown in b) indicating the optimal arrangement of residues and the intra hydrogen bond. In c) the 3D structure of GS shows the hydrophobic side (top) and hydrophilic side which make up the amphipathic structure of the GS monomer. The low energy GS structure is courtesy of M. Rautenbach and was modelled utilising Yasara 11.3.2 and its crystal structure reported by Saiz et al.<sup>21</sup>

## 2. METHODS

### 2.1. Materials

GS (>99% purity as determined with mass spectrometry) was purchased from Sigma Aldrich (St. Louis, MO, USA). 1-octanol (≥99%, 1-octanol) was purchased from Sigma Aldrich (Gillingham, UK) and used without further purification.

### 2.2. Sample preparation

A volume of 30 μL of a solution of GS in 1-octanol at a concentration of 5 mg/mL (4.38 mM) was prepared and contained between two calcium fluoride (CaF<sub>2</sub>) windows separated by a 50 μm polytetrafluoroethylene (PTFE) spacer and housed in a temperature-controlled transmission (Harrick) cell accurate to ±1 °C, for temperatures between 20 – 80 °C. For analysis purposes, a solution of 1 mg/mL (876 μM) was also prepared and measured using 2D-IR.

### 2.3. FTIR spectroscopy

FTIR absorption spectra were obtained using a Bruker Vertex 70v spectrometer with a resolution of 1.0 cm<sup>-1</sup> and each acquired FTIR spectrum was an average of 20 co-added scans in the spectral range 400 - 4000 cm<sup>-1</sup>. At each temperature measurements were done in triplicate and the spectra presented is the average.

### 2.4. 2D-IR spectroscopy

2D-IR measurements were acquired using the Lifetime (100 kHz) laser system at the STFC Rutherford Appleton laboratory, using a methodology that has been described elsewhere.<sup>22,23</sup> Briefly, the experiment is based on three mid-IR laser pulses arranged in a pump-probe geometry. The first two pump pulses, which are separated by time,  $\tau$ , interact and excite the sample; therefore the excitation or pump frequency axis results from Fourier transforming the signal as a function of the time delay between the two pump pulses. The timing between the two pulses can be controlled and varied by use of a pulse shaper. The third pulse which is the probe pulse which follows after a waiting time,  $T_w$ , interacts with the sample resulting in emission of a signal, known as the photon echo, after a time,  $t$ . This signal is emitted in a direction collinear with the probe pulse, it is self-heterodyned. When this signal is spectrally dispersed via a diffraction grating then proceeds onto a liquid nitrogen cooled detector array which forms the probe axis of the 2D-IR spectrum with a spectral resolution of 1.5 cm<sup>-1</sup>.<sup>24-26</sup> 2D-IR spectra were recorded at  $T_w$  values of 250 fs, using parallel pump-probe polarization relationship. Signals are averaged for 50 000 shots, which at a repetition rate of 100 kHz, meant that measurements can be done in a minute.<sup>23</sup>

### 2.5. Infrared spectroscopy data analysis

At each temperature, the solvent spectrum was subtracted from the GS solution spectrum, ensuring that only temperature changes to the peptide are measured. FTIR and 2D-IR absorption spectra were also analysed using difference spectroscopy and principal component analysis (PCA), with PCA available from Origin 2018b. For temperature studies, difference spectra were obtained by subtracting the spectrum at 20 °C (native state) from the spectrum at elevated temperatures to obtain thermally induced structural

changes of the peptide from its native state. The use of 2D-IR difference spectra is standard<sup>27,28</sup> and the need for phasing is removed by use of pump-probe geometry which collects phasing and non-rephasing spectra simultaneously. In 2D-IR, pulse shaping assists further in terms of pump-pulse phase control. Fluctuations are dealt with by averaging, which is improved significantly in pulse high repetition rate laser systems like Lifetime (100 kHz) laser system and ULTRA at the STFC Rutherford Appleton laboratory<sup>29–33</sup>.

Data was normalised to the maximum intensity to eliminate minor fluctuations due to electronic noise, sample variation and signal intensity. Normalisation of spectra was performed as a standard, using peak maxima, irrespective of frequency. Normalising with respect to peak maxima or at constant frequency gave comparable and, in some cases, similar results, by analysing the integral area under the curve for both methods [Figure S-1](#). Band profiles were checked similarly, and they did not change significantly with the peak intensity variations indicating that our approach of normalising was valid in order to compare data sets.

PCA was performed after solvent subtraction and normalisation. PCA as used in our analysis shows variance and identifies spectral differences and it does not provide anything specifically chemical/structural. PCA was applied to scrutinise the data and identify variations between data sets. The use of PCA is well established in spectral analysis to provide a means to make visualisation of spectral differences easier where differences in spectral profiles are observed and where the modes showing differences can be assigned and can provide first insights into possible differences in molecular structure to focus on in drawing up hypothesis. Standard second (2<sup>nd</sup>) derivative spectral analysis was performed and is explained in [Supporting Information](#).

## 2.6. Simulation of a GS trimer model and QM/MM simulations

A GS trimer model was considered for QM/MM simulations to represent GS at high concentration [Figure S-2b](#). A GS monomer model with two intact  $\beta$ -turns and an intact intramolecular antiparallel  $\beta$ -sheet was derived from X-ray structures with reference to crystal structure reported by *Saiz et al.*<sup>21</sup> [Figure S-2a](#). Modelling of the GS structure was done utilising YASARA version 11.2.18 (YASARA Biosciences GmbH, Vienna, Austria, [www.yasara.org](http://www.yasara.org)<sup>34</sup>). A YASARA protocol from *Rautenbach et al.*<sup>35</sup> was utilised to create a low energy  $\beta$ -sheet type GS dimer and trimer. The protocol entailed molecular docking followed by mechanistic molecular dynamic simulations to remove conformational stress and test stability of the selected low energy  $\beta$ -sheet type GS dimer and GS trimer.

Spectral simulations of the infrared absorption on the model GS trimer were performed using Gaussian 09 package made available through the Centre for High Performance Computing in Cape Town was used for the calculations. In the simulations, quantum mechanical/molecular mechanics (QM/MM) level of theory accounted for neighbour-neighbour interactions and the influence of H-bonding on the eigenmodes obtainable from the peptides, which was implemented through the ONIOM framework available in

Gaussian 09. Relative to the experimental spectra, the best ONIOM framework for the exchange-correlation energy/basis set was found to be B3LYP/6-31g(d,p):UFF. The GS structure was subjected to simultaneous optimisation of the atomic redundant coordinates and frequency calculations for the infra-red spectra. Octanol as a solvent was modelled through the framework of polarizable continuum model (PCM) with a dielectric constant of 9.86. The force field and the cavity provided by the solvent ensured stability and electronic charge balance during optimization and the subsequent vibrational frequency calculation. The bulkiness of the structure required a solvent in-order to get reasonable results. The solvent was also a guide to replicating real life solvent-solute hydrogen bonding interactions. The calculations were done progressively from a monomer to a trimer to mimic the concentration level used in the experiment and to see other interactions between the QM and MM structural ensembles.

Band assignments of vibrational modes in the trimer model spectra were done by visually observing the structural groups and modes of vibration using GaussView 5 software and assigning to the spectral feature which the vibrating mode contributes to. Viewing the vibrating modes in GaussView 5 software enabled the assignment of the calculated peaks with the contributing amino acid. In the QM/MM simulations a trimer model was chosen because we expect stacks to be present at the GS concentrations used in the experiments. For the QM/MM simulations we wanted to consider the influence of constraining the motion of a single peptide in space, and a trimer model is the smallest structure to accomplish this.

## 3. RESULTS

### 3.1. FTIR Absorption Spectroscopy

The infrared absorption spectrum of GS in 1-octanol features a broad band centred at 1645  $\text{cm}^{-1}$ , which can be assigned to the amide I mode. As the temperature was increased from 20 - 80 °C, the peak maximum shifted to 1647  $\text{cm}^{-1}$  [Figure 2a](#), however, this was not due to a simple change in frequency of the band as an isosbestic point is observed at 1650  $\text{cm}^{-1}$ .

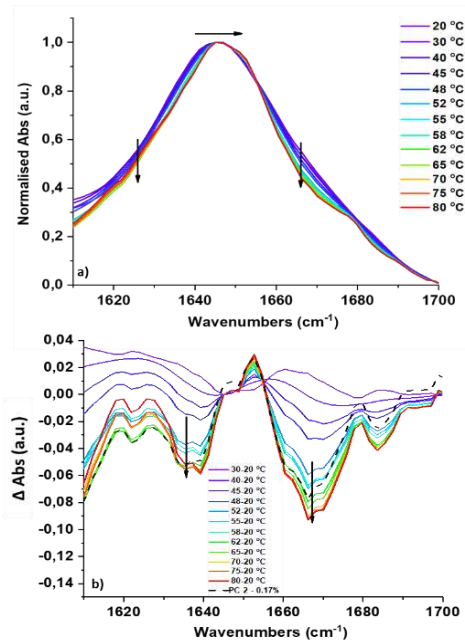


**Figure 2.** (a) FTIR absorption spectra of the amide I region of 5 mg/mL GS in 1-octanol measured over the temperature range 20 – 80 °C. The spectra were solvent subtracted and an average from triplicate measurements. (b) Difference spectra obtained by subtracting the normalised spectrum at 20 °C from normalised spectra obtained at elevated temperatures. The black dashed line shows the PC 2 contribution obtained following PCA.

Difference spectra calculated relative to the spectrum of GS at 20 °C [Figure 2b](#), showed that at elevated temperatures a reduction in absorption intensity from the amide I band occurs near 1645  $\text{cm}^{-1}$  and at 1666  $\text{cm}^{-1}$ . The spectral features near 1620  $\text{cm}^{-1}$  and at 1680  $\text{cm}^{-1}$  observed at elevated temperatures [Figure 2a](#) are consistent with those expected from the amide I mode of an antiparallel  $\beta$ -sheet structure <sup>36–38</sup>. The feature appearing near 1620  $\text{cm}^{-1}$  is consistent with bands which appear in the presence of aggregation <sup>39,40</sup>.

The temperature-dependent spectroscopy data was inspected further using PCA. The total variance is well represented by two principal components, PC 1, correlating to 99.8 % of the total variance, was found to be invariant with temperature, while the minor contribution of PC 2 (0.2 %) varied with temperature. Although the PC 2 contribution is minor, features of the spectral distribution of PC 2 correlated well to those observed in the difference spectra (black spectrum [Figure 2b](#) and [Figure S-3](#). Features of PC 1 obtained using Gaussian fitting of the IR spectra also correlated well with the FTIR spectra [Figure S-4](#).

### 3.2. 2D-IR Spectroscopy of GS in 1-octanol

2D-IR spectra measured at temperatures between 20 °C and 80 °C are shown in [Figure S-5](#). At 20 °C the 2D-IR spectrum of GS in 1-octanol features a positive peak (red) located on the diagonal at a pump and probe frequency of 1650  $\text{cm}^{-1}$ , which is assigned to the  $\nu = 0 - 1$  transition of the amide I mode of GS [Figure 3a](#). A negative off-diagonal peak assigned to the accompanying  $\nu = 1 - 2$  transition is located at the same pump frequency (1650  $\text{cm}^{-1}$ ) but a probe frequency of 1635  $\text{cm}^{-1}$ . This peak is shifted along the probe axis direction by the anharmonicity of the amide I mode. By fitting two

Gaussian functions to each of the slices taken through the 2D-IR spectrum at pump frequencies of 1640, 1650 and 1660  $\text{cm}^{-1}$  showed that the anharmonic shift of the amide I band was not constant, with shift values of 16, 16 and 13  $\text{cm}^{-1}$  obtained at each pump frequency, respectively [Figure S-8](#). In [Figure S-8](#), a third Gaussian was fit to the slice at 1660  $\text{cm}^{-1}$  at 20 °C and this did not change the profile.

At 80 °C, the diagonal peak  $\nu = 0 - 1$  transition was present at pump and probe frequencies of 1651  $\text{cm}^{-1}$  while the off-diagonal  $\nu = 1 - 2$  transition was located at probe frequency 1636  $\text{cm}^{-1}$  [Figure 3b](#). Again, for slices taken at pump frequencies of 1640, 1650 and 1665  $\text{cm}^{-1}$  at high temperature, the anharmonic shift at each of the same three pump frequency positions was observed to increase to non-constant anharmonic shifts of 21, 19 and 16  $\text{cm}^{-1}$ , respectively. These shifts indicate a progressive change in the anharmonicity which can be ascribed to complex bands with more than one underlying contribution. The smaller anharmonicity values observed at the lower temperature are completely consistent with a greater degree of coupling in the system because large coupled secondary structure units show smaller anharmonicity, which is consistent with our assignment to loss of intermolecular interactions at high temperature <sup>25</sup>.

An off-diagonal peak with a pump frequency of 1650  $\text{cm}^{-1}$  and a probe frequency near 1660  $\text{cm}^{-1}$  was observed in the 2D-IR spectrum of GS at 20 °C [Figure 3a](#). This feature disappeared as the temperature was raised to 80 °C [Figure 3b](#). Difference 2D-IR spectra obtained as a function of temperature are shown in [Figure S-6](#). The overall difference 2D-IR spectrum 80 – 20 °C, [Figure 3c](#) shows three distinct peaks, all with a pump frequency close to 1650  $\text{cm}^{-1}$ . An intense positive peak is located at a probe frequency of 1646  $\text{cm}^{-1}$  (red arrow), while two negative peaks occur at probe frequencies of 1613  $\text{cm}^{-1}$  (blue arrow) and 1666  $\text{cm}^{-1}$  (black arrow). Using this difference spectrum representation, the negative peak at a probe frequency of 1666  $\text{cm}^{-1}$  indicates a reduction in intensity of the (positive)  $\nu = 0 - 1$  signal between 20 and 80 °C. This is likely to be due to the combined effects of a reduction in overall peak intensity and the loss of the off-diagonal feature located at pump, probe position 1650, 1660  $\text{cm}^{-1}$  with increasing temperature. The positive peak at 1646  $\text{cm}^{-1}$  indicates a reduction in size of the negative  $\nu = 1 - 2$  peak identified above. Finally, the feature at 1613  $\text{cm}^{-1}$  (orange arrow) is indicative of an increase in the  $\nu = 1 - 2$  peak. The latter two observations are consistent with the observed increase in anharmonicity at higher temperatures, which shifts the negative  $\nu = 1 - 2$  peak to lower probe frequencies [Figure 3c](#).

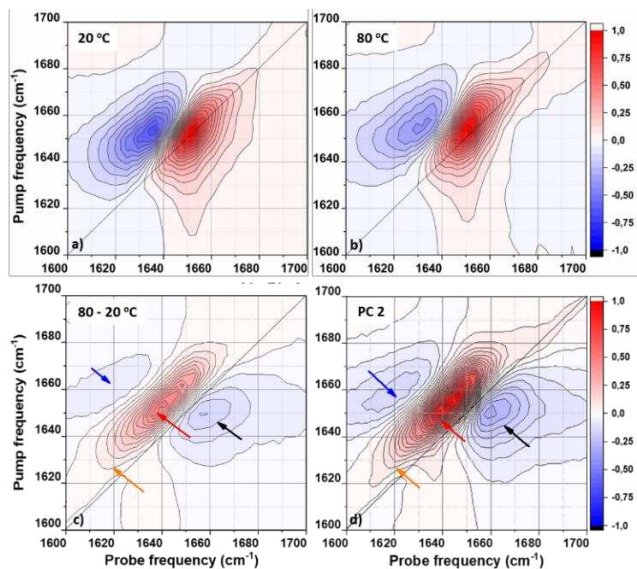


**Figure 3.** 2D-IR spectra of GS in 1-octanol averaged from triplicate measurements at (a) 20 °C and at (b) 80 °C. The 2D spectra denoted 80 - 20 °C (c) is the difference spectra showing the temperature induced changes between 20 and 80 °C, and (d) is the PC 2 spectral distribution showing spectral signatures similar to those in the difference spectra. Arrows indicate specific spectral features discussed below.

Applying PCA to the 2D-IR data revealed that two PCs were required to describe 99.9% of the observed variance. PC 1 (96.2 %, Figure S-7a) was temperature independent and contained the larger part of the variance while PC 2 (3.7 %, Figure 3d) showed a strong temperature dependence. The spectral distribution of PC 1 resembled the average 2D-IR spectrum for all temperatures Figure S-7b, while PC 2 showed temperature dependent variations very similar to those described in the difference spectra Figure 3d. Given the close agreement between results obtained from analysis using difference spectroscopy and PCA, further interpretation focussed on the PCA results alone. The fact that the data can be represented by only two PCs suggests that the changes observed are not spurious but are related to reproducible structural changes.

For the 1D absorption spectra in Figure 2 below three consecutive temperature ramp measurements were made on each sample, giving a standard deviation of area under the absorption curve within  $\pm 1.7$  %. Furthermore, 3 different samples were measured each with a fresh peptide sample and spectra were reproducible within  $\pm 3.9$  %. Likewise, for 2D-IR, measurements were repeatable within  $\pm 2.0$  % and reproducible within 6.1 %. For spectra measured at 20 °C before heating and another measured after cooling back to 20 °C, spectra differed by  $\pm 2.3$  %. In general, data from samples is normalised to account for variations arising from the sample path length, laser intensity and concentration of the sample, but reproducibility in both 1D and 2D from sample-to-sample may present larger errors as it is harder to reproduce absolute concentrations in different samples. Additionally, the use of PCA is advantageous in noise reduction, as variations from random instrumental or sample-related noise will be in other PCs which are not the first two PCs.

### 3.3. QM/MM simulations

Band assignments were obtained by visualising the vibrational modes from the calculated spectra in GaussView 5 software for the GS trimer model. Between 1670 - 1700  $\text{cm}^{-1}$ , the amide I mode, a few strong vibrations were observed Figure 4.

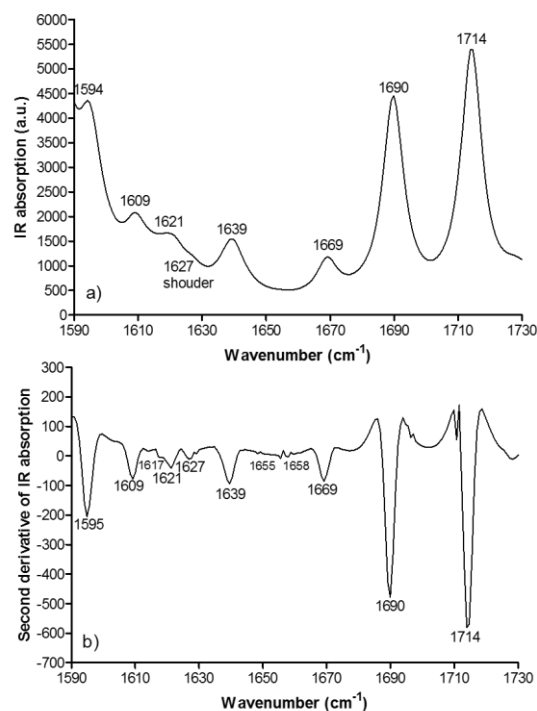


**Figure 4.** IR spectra for GS trimer model in octanol simulated using QM/MM calculations with assigned bands contributing to amide I mode, with (a) the simulated IR spectrum and (b) the 2<sup>nd</sup> derivative spectrum. The labelled bands are allocated in Table 1, as identified using the GaussView software.

There was a good correlation of bands observed for GS in octanol (experiment) and the GS trimer model as determined with GaussView. (Table 1, Figure 4, Figure S-9). The bands at 1669  $\text{cm}^{-1}$  and 1690  $\text{cm}^{-1}$  in the model and 1670  $\text{cm}^{-1}$  and 1685  $\text{cm}^{-1}$  (experiment) are attributed to by carbonyl (C=O) stretch of the  $\beta$ -turns, which is vibrationally coupled (anharmonic coupling) to the Orn amino side chain. Orn is one of the residues in the two identical  $\beta$ -turns. At 1634  $\text{cm}^{-1}$  bands from the  $\beta$ -sheet carbonyls were also experimentally observed and this band is observed at 1639  $\text{cm}^{-1}$  in the GS trimer model in octanol. Bands from  $\beta$ -sheet and NH bending modes at 1652-1658  $\text{cm}^{-1}$ , also correlated between the GS trimer model and experimental spectra. Good correlation bands at 1616, 1626 and 1608/9  $\text{cm}^{-1}$  in octanol and was linked to C-C stretch of Phe. A prominent vibration at 1714 (model) and 1717  $\text{cm}^{-1}$  (experiment) was attributed to C=O stretch of the Pro amide I. The proposed band assignments of GS in Table 1 are also in general agreement with GS literature<sup>41</sup> and those which have been made from DFT calculations on dipeptides<sup>42</sup> and other compounds such as methylacetamide and polycyclic aromatic hydrocarbons.<sup>43,44</sup>

## 4. DISCUSSION

### 4.1. Extent of vibrational coupling

To gain a deeper insight into changes in secondary structure occurring within the GS system, we combined the results of linear

absorption and 2D-IR measurements as a function of temperature to extract transition dipole spectra. This follows the approach first devised by Grechko and Zanni<sup>45,46</sup> and adapted by Minnes *et al.*<sup>33</sup> for temperature dependent studies of secondary structure. The method uses the premise in linear spectroscopy that the size of the amide I absorption band of a given system is independent of changes in vibrational coupling because the signal scales as the transition dipole moment squared ( $|\mu|^2$ ). In contrast, for 2D-IR spectroscopy, the transition dipole moment scales as ( $|\mu|^4$ ) and so the size of the diagonal peak will change to reflect changes in transition dipole moment caused by modified couplings.<sup>45-47</sup> This can be envisaged through the ratio of the signal of 2D diagonal spectrum shown in Figure 5b and the IR absorption spectrum in Figure 5a in the amide I region, where, the 2D diagonal signal increases relative to that of the FTIR when there is an increase in vibrational coupling.<sup>33</sup>

The relative changes in transition dipole moment, denoted as  $d(\omega)^{rel}$ , with reference to the initial temperature of 20 °C were obtained using the following equation (1):

$$d(\omega)^{rel} = \frac{2D-IR_T(\omega) OD_{20}}{FTIR_T(\omega) \Delta OD_{20}} \quad (1)$$

Where  $d(\omega)^{rel}$  represents the 'spectrum' of the relative transition dipole strength and is a function of frequency,  $\omega$ .  $2D-IR_T(\omega)$  and  $FTIR_T(\omega)$  are functions of frequency ( $\omega$ ) for the absolute values of the 2D diagonal and the 1D absorption spectral signals, respectively, at different temperatures (T).  $OD_{20}$  and  $\Delta OD_{20}$  are the maxima of the 1D absorption spectrum and the 2D diagonal signal, respectively at T

= 20 °C which in this case is the reference temperature. The results of the transition dipole analysis are shown in Figure 5c. The calculated integral area for the amide I peak in the linear absorption spectrum did not change as the temperature increased, as expected. However, that of the 2D diagonal decreased strongly with increasing temperature, as shown in Figure 5d.<sup>46</sup> The calculated transition dipole spectra reflect these effects via a significant decrease in intensity of the transition dipole spectra between 20 and 80 °C in Figure 5c. This is consistent with observations derived from the difference spectra in 2D-IR analysis presented above, which showed reduction in the size of the  $\nu = 0 - 1$  peak amplitude over the same temperature range.

Examining the transition dipole spectrum in more detail, the observed decrease in intensity is focused upon the 1630  $\text{cm}^{-1}$  to 1660  $\text{cm}^{-1}$  region which encompasses the lower frequency portion of the amide I band, though changes in the transition dipole strength are observed right across the region studied. This strongly indicates that with increasing temperature, the strength of vibrational coupling of the elements linked to the amide I band of GS decreases and this is evidenced in the observed spectrum in Figure 5c<sup>46,48,49</sup> Such observations have previously been attributed to loss of secondary structure or self-association in protein and peptides and could be consistent with loss of inter or intra-molecular interactions of GS. The decrease in coupling at high temperature is also consistent with the observed increase in anharmonicity, which scales inversely with the extent of coupling in secondary structures<sup>45,46</sup> as well as the disappearance of the off-diagonal peak illustrated in Figure 3d.

**Table 1** Summary of simulated GS amide I spectra in octanol and experimental FTIR amide I spectra for 1 and 5 mg/mL GS in octanol. Wavenumbers are shown in  $\text{cm}^{-1}$ , numbers in brackets have peaks only in 2<sup>nd</sup> derivative spectra at all concentrations, \* and # indicated linked vibrational modes, numbers in italics have ambiguous assignments to two modes. The model spectrum and 2<sup>nd</sup> derivative spectrum from which the model data were derived can be found in Figure 4. The experimental spectra and 2<sup>nd</sup> derivative spectra from which the data were derived can be found in Figure S-9.

Structure or amino acid	Absorbing Group	Literature Models <sup>a-e</sup>	GS <sup>f</sup>	GS/Octanol Trimer model <sup>g</sup>	GS/Octanol Experimental
Pro	C=O stretching (amide I)			1714	1717
		1700	1700		1699 (1701, 1705)
$\beta$ -sheet	Stretching C=O (amide I)	1695-97			1696
		1691-93		1690 <sup>#</sup>	
		1641-43	1643		(1642)
		1630-39		1639	1634, 1636
$\beta$ -turn	Stretching C=O (amide I)	1624-29			
		1683-91		1690 <sup>#</sup>	1685
		1678-82			1682
		1670-75			1674, 1676
		1666-74		1669 <sup>*</sup>	1670
		1659-65	1655	(1655)	1652, 1653, 1656
	1654-58				
	1672-73				

Orn	Bending	-		1690 <sup>#</sup>	1685
		1667		1669*	1670
	NH <sub>3</sub> <sup>+</sup>	1660			
	(amide I)	1659		(1658)	1656
		1647			1645, 1647
	Stretching	-		(1617)	1616
Phe	C-C (ring)	-		1621	1626
				(1626)	
	(amide I and II	1602	1601	1595	
				1609	1608

<sup>a</sup> Krimm *et al.* (1983); <sup>b</sup> Venyaminov & Kalin (1990); <sup>c</sup> Barth (2007); <sup>d</sup> Barth (2000); <sup>e</sup> Kong *et al.* (2007); <sup>f</sup> Naik *et al.* (1984)

At 20 °C, the linear absorption spectra for GS in [Figure 5a](#) highlights the main peak near 1645 cm<sup>-1</sup> and a high frequency peak near 1670 cm<sup>-1</sup>, which is indicative of  $\beta$ -sheet and  $\beta$ -turn structures, respectively. The cross peaks observed in two-dimensional spectra in [Figure 3](#) are also an indication of the presence of antiparallel  $\beta$ -sheets <sup>36,50,51</sup>. The shifting of the strong absorption band to higher energy, from 1645 – 1647 cm<sup>-1</sup> suggests  $\beta$ -sheet structures <sup>39,50</sup>. At the 80 °C, weak peaks appear in the FTIR absorption spectra near 1620 and 1680 cm<sup>-1</sup>. However, these peaks in [Figure 5b](#) are not strongly represented in the two-dimensional spectra.

Peptide structure calculations have been done on GS in gas phase and three GS conformers have been highlighted <sup>39,40</sup>. These conformers mainly result from interactions of Phe chromophores which are weakly coupled to each other, and Phe chromophores which interact strongly with charged Orn side chains. Furthermore, the structures are dominated by side chain-backbone coordination of the -NH<sub>3</sub><sup>+</sup> group from the charged Orn side chains and the backbone Phe C=O group. It is further explained that the amide I band maxima band position is influenced by solvents of different polarity, and the spectral signatures depend on the environment. In condensed phase, a band position of 1633 cm<sup>-1</sup> is suggested for  $\beta$ -sheets which are embedded in large networks; 1640 cm<sup>-1</sup> for  $\beta$ -sheet sections which interact with polar solvents; and 1616 cm<sup>-1</sup> a band which appears when aggregation occurs <sup>39,40</sup>. From our results, the structure of GS is considered in condensed phase, and it is influenced by three factors; concentration, temperature and solvent environment. At 5 mg/mL GS is probably aggregated while in solution with octanol. The influence of heat in the considered temperature range does not, in this case, denature the peptide, but only maximises the disruption of the GS aggregates. From our result we can highlight three conformers contributed to the main band from  $\beta$ -sheet structures centred near 1645 cm<sup>-1</sup>, a high frequency peak near 1670 cm<sup>-1</sup> from  $\beta$ -turns and the 1620 cm<sup>-1</sup> peak which can be attributed to presence of aggregated structures <sup>39,40</sup>. In addition, since the main absorption band is not shifting to lower energy <sup>50</sup> and the heating process was reversible, it indicates that extended sheets are not present in the system, and if present, their signal contribution would be minimal as these may only be represented by a small fraction of the bulk GS. This data and that of PCA show consistent differences.

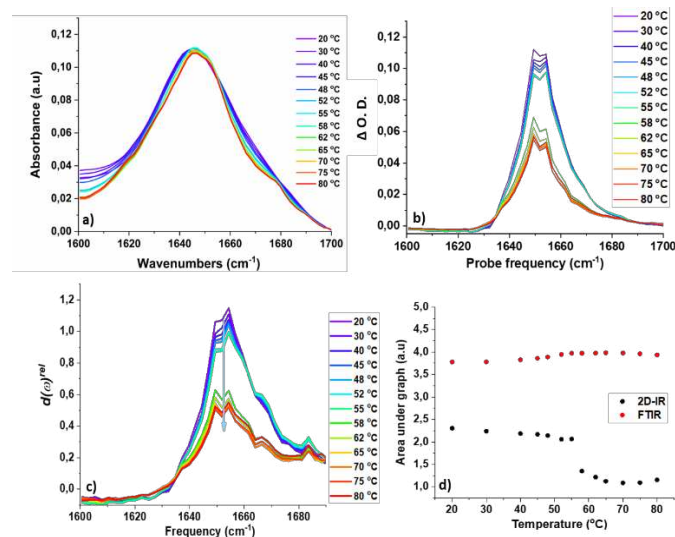


**Figure 5.** Comparison of FTIR and 2D-IR spectra that were plotted for GS in 1-octanol from 20 - 80 °C. (a) is the FTIR absorption spectra (b) are the 2D-IR diagonals (absolute values from raw data) and (c) shows the calculated  $d(\omega)_{rel}$  spectra, (d) shows the integral area under the graphs for 1D and 2D. Data points for area under graph in for FTIR in (d) are averages from the triplet measurements done at each temperature. The error bars indicate the variation in the area at each temperature.

#### 4.2. Temperature profile of GS in 1-octanol

From the analysis above, the increase in anharmonicity which correlates with an observed loss of coupling shows that changes in GS are consistent with a loss either of oligomers/aggregates and/or intramolecular hydrogen bonding at elevated temperature. In this section we focus on the temperature profile of these changes in order to shed more light on the molecular origins of the spectroscopic changes. Both PCA and difference spectroscopy analyses indicated the reduction in size of the  $v = 0 - 1$  peak of GS at (pump, probe) frequencies of (1650, 1666 cm<sup>-1</sup>) in the 2D-IR data. This can be attributed to the effects of reduced coupling on modes contributing to the amide I profile, and the loss of an off-diagonal peak observed in the 2D-IR spectrum at 20 °C. Examining the temperature dependence of this feature shows that the changes are gradual from 20 - 55 °C but with a significant loss in amplitude occurring above 55 °C, depicted in [Figure S-6](#).

The results of PCA were used to produce a thermal profile for the temperature-dependent component (PC 2) determined for each of the IR absorption in [Figure 6a](#) and 2D-IR studies in [Figure 6b](#).

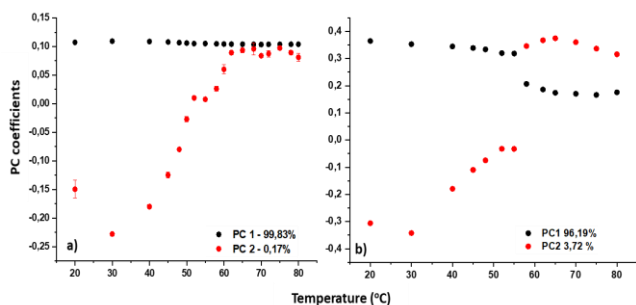


**Figure 6.** PC 1 and PC 2 coefficients vs temperature for a) FTIR and b) 2D-IR. Both the PC2 profiles show thermal induced changes from PCA analysis on the FTIR and 2D-IR data. The error bars in the data sets indicate the variation in the area at each temperature from the average triplicate measurements.

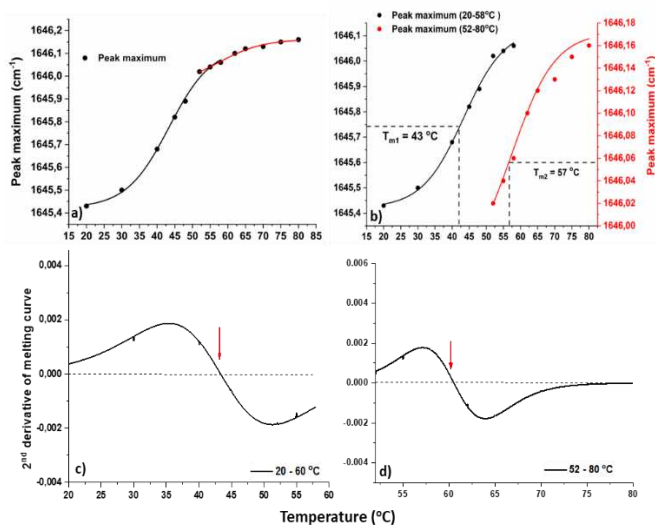


**Figure 7** Melting curves (Boltzmann sigmoidal profiles) of the peak maxima shift of the main infrared absorption band near  $1645\text{ cm}^{-1}$ . Band positions were obtained from the 1<sup>st</sup> derivative spectra, and are in Table S-1. In a) is the melting curve for temperature range 20 - 80 °C showing the two profiles and in b) the separate profiles are shown more clearly; for the transition from 20 - 58 °C with  $T_{m1} = 43 \pm 2\text{ °C}$  (black) and the transition 52 - 80 °C with  $T_{m2} = 59 \pm 2\text{ °C}$  (red). Spectra c) and d) are 2<sup>nd</sup> derivative profiles for the melting curves in b) with arrows indicated the said melting temperatures.

This approach confirms the two transition temperatures near  $43 \pm 2\text{ °C}$  and  $59 \pm 2\text{ °C}$  for both FTIR and 2D-IR, and changes follow a bimodal profile. Additionally, from an analysis of the band maxima position for the infrared absorption spectra in Figure 7a, again two transition temperatures are evidenced from fitted melting curves in Figure 7b. From the Boltzmann sigmoidal melting curves, the corresponding 2<sup>nd</sup> derivative spectra in Figure 7c and d showed the transition temperatures  $T_{m1} = 43 \pm 2\text{ °C}$  and  $T_{m2} = 59 \pm 2\text{ °C}$ , confirming the 2D-IR and PCA results.  $T_{m2}$  was also further defined using area under the 2D-IR diagonal curves and was obtained as  $57 \pm 2\text{ °C}$  from fitted melting curve in Figure S-10.

Although both FTIR and 2D-IR data highlight the same two transitions, only the 2D-IR spectral response is sensitive to changes in vibrational coupling. It is therefore interesting that the second transition temperature in range 57 - 60 °C dominates in the PC 2

profile of the 2D-IR data in Figure 6b whereas the lower temperature transition appears more dominant in the FTIR data in spectra of Figure 7. Taken together, this suggests a greater loss of coupling at high temperature. However, the presence of two transitions in both FTIR and 2D-IR show that the molecular changes do influence both measurements, as would be expected. Furthermore, the fact that both transitions appear in a single PC, indicate that they have similar spectroscopic origins and therefore a similar molecular interpretation. We therefore conclude that the loss of coupling observed in the 2D-IR spectrum at higher temperature is associated with redistribution of oscillator strength in the FTIR data, whereas the lower temperature transition leads to changes in both datasets, but with a lesser emphasis on loss of coupling. The cross peak observed in the 2D-IR spectrum at 20 °C of Figure 3a shows that the bulk of the non-covalent structural elements that we are observing in the amide I region is the C=O vibrations of  $\beta$ -sheets (inter- and intrapeptide H-bond) and the intrapeptide  $\beta$ -turns. Therefore, we attribute the first melting transition,  $T_{m1}$ , to changes in interpeptide H-bonding within aggregates/oligomers undergoing partial dissociation to smaller oligomers. These oligomers can then undergo further dissociation to monomeric structures as the dominant structure during the second melting transition. The monomeric GS structure only has intrapeptide  $\beta$ -sheet and  $\beta$ -turn hydrogen bonds in its structure, as is also indicated by the shifts in the relevant amide bands. Simulations for monomeric GS are illustrated in Figure S-11. From the profiled dissociation process of aggregated/oligomeric GS, transitions can be identified within two temperature ranges; at 40 - 55 and 48 - 80 °C.  $T_{m1}$  was identified as  $45 \pm 2\text{ °C}$  from Figure 6a;  $41 \pm 2\text{ °C}$  from Figure 6b and  $43 \pm 2\text{ °C}$  from Figure 7b. This gave a broad range of values from 41 - 47 °C for  $T_{m1}$  from data obtained from different methods.  $T_{m2}$  was calculated as  $59 \pm 2\text{ °C}$  from Figure 6, Figure 7b, Figure S-10 as well from the transition dipole spectra. Overall, even though there are slight discrepancies in the exact temperatures of the transitions and that the different analysis methods show the transitions to different degrees, it seems reasonable to conclude that both spectroscopy experiments are reflecting the same molecular changes and the two transitions are unequivocal.

In an aqueous solution, the GS aggregation/oligomerisation process is driven by hydrophobic forces due to the amphipathic nature of the molecule.<sup>20,52</sup> The GS monomers cluster in a such a way that the hydrophobic groups face each other, reducing their exposure to polar solvent groups/molecules and assembling into larger structures.<sup>53-56</sup> Hydrophobic residues in GS such as Leu and Val lack repulsive electrostatic interactions and cluster through Van der Waals interactions,<sup>54</sup> while aromatic residues such as Phe can partake in aromatic stacking stabilised by London dispersion forces. However, as in the experiments reported here, in the more non-polar 1-octanol, hydrophobic interactions will be dispersed by the hydrophobic octanol tail, limiting hydrophobic clustering. Conversely, inter- and intrapeptide hydrogen bonds will be supported as there will be less competition for hydrogen bonds and dipole-interactions in octanol than in water. The inter-peptide

hydrogen bonds are lost at increasing temperature, as shown from our results.

$T_{m1}$  was more evident from the PC 2 of FTIR absorption spectra. This melting point could be related to the loss of hydrogen bonded oligomers, loss in interactions with the Orn amino group, as well as loss of aromatic stacking of Phe, summarised in Table 2. The role of Phe in oligomerisation has been illustrated by Helle *et al.*<sup>20</sup> and in the study, the UV absorption at 257 nm decreased over time and with the increase in concentration. This indicated that Phe groups were either exposed to a polar environment or have polar interactions with the Orn residues or Phe-Phe stacking interaction in the oligomer/aggregates in this study. The spectroscopic response of the system changes after  $T_{m2}$  and is better described by the 2D-IR analysis of GS in octanol. Changes in intramolecular structure occurs at  $57 \pm 2$  °C whereby conformations with hydrogen-bonds, such as inter-peptide H-bonds and the two intra-peptide  $\beta$ -turns and antiparallel  $\beta$ -sheet are either revealed or melted away. Structures, which were buried/observed in aggregates/oligomers, emerged with the increase in temperature.  $T_{m2}$  could therefore relate to the demasking of intra-peptide structures by loss of interpeptide interactions. FTIR as well as 2D-IR analysis indicated that changes in  $\beta$ -sheet structures occur at  $T_{m2}$ .

Second derivative spectral analysis has been extensively used as a data analysis method in protein and peptide studies.<sup>57,58</sup> Peaks identifiable in a 2<sup>nd</sup> derivative spectra of FT-IR absorbance spectra can be assigned to the secondary structures in the region of amide I, II and III following reference data<sup>59–62</sup> and significant information can be obtained on the stability and structural details of proteins and peptides in various environments.<sup>61</sup> Results from the 2<sup>nd</sup> derivative analysis in Figure 8 confirmed the structures identified from the infrared spectral simulations and could be compared, as well as discussed according to Figure 9.

$T_{m1}$  uncouples the C=O groups of the  $\beta$ -sheets and turns in the smaller oligomeric structures. In Figure 9 and Table 2 there is significant decrease in C=O stretch vibrations of  $\beta$ -sheets at 1642 and 1650  $\text{cm}^{-1}$  near 45 °C. There is loss of C=O stretching of the  $\beta$ -sheet at 1642  $\text{cm}^{-1}$ . There is loss of C=O stretch vibration of  $\beta$ -sheets near 1650  $\text{cm}^{-1}$  at a higher  $T_m$  of 45 °C, which also exhibited as an off-diagonal peak in 2D-IR. We relate this to loss of interpeptide H-bonding, resulting in smaller more stable oligomers. Equally, there is an increase in C=O stretch vibrations of  $\beta$ -sheets at 1696 and 1699  $\text{cm}^{-1}$  around 45 °C, as well as those of the  $\beta$ -turns at 1685  $\text{cm}^{-1}$ . At high concentration, the vibrations of these structures increases and at high temperature, the decrease in vibration suggests disruption of some of the  $\beta$ -sheet structures vibrating at the lower wavenumbers, implying that the carbonyl groups are possibly involved in intrapeptide oligomers/aggregates. This will be further illustrated in section 4.3.

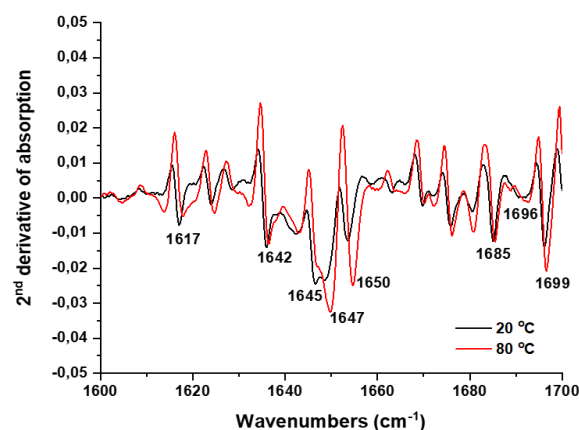


**Figure 8** The 2<sup>nd</sup> derivative spectra of the two extreme temperatures 20 °C and 80 °C, showing wavenumbers ( $\text{cm}^{-1}$ ) of the prominent peaks related to the prominent peptide structures. Spectra from 20 – 80 °C are shown in Figure S-12.

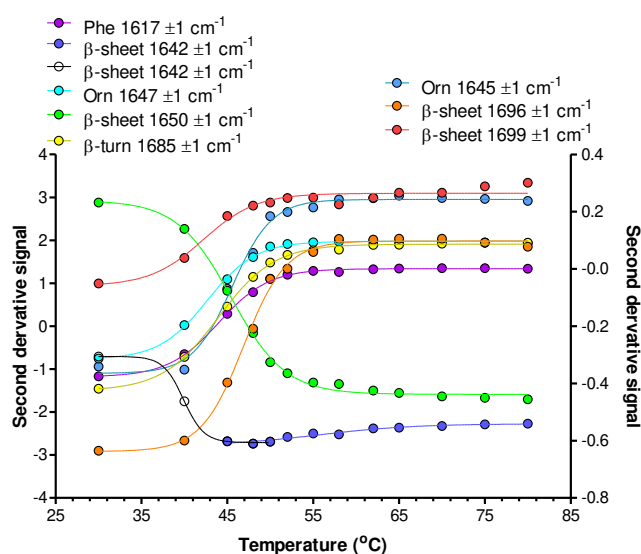


**Figure 9.** Melting curves of spectral structure components present in GS at 5.00 mg/mL solution, identified in Figure 8 and summarised in Table 2. The melting temperature ( $T_m$ ) was determined for each curve using an adapted Boltzman sigmoidal curve fit to the following equation:  $Y = \text{Lowest signal} + (\text{Highest signal} - \text{Lowest signal}) / (1 + \text{signal}((T_m - X)/\text{Slope}))$ . All curve fits were  $R^2 \geq 0.97$ . The axis on the left is for the data with legend on the left and the axis on the right is for the data with legend on the right.

### 4.3. Further analysis and discussion on the effects of concentration and temperature on structural changes

To compare the effect of concentration and the effect of temperature induced structural changes, 1D absorption and 2D-IR spectra of a 1 mg/mL sample of GS in 1-octanol were taken under the same experimental condition at 20 °C, shown in Figure S-13. Structural changes which occur with increasing concentration from 1 - 5 mg/ml are narrowing and shifting of the band maxima from 1649  $\text{cm}^{-1}$  (1.00 mg/mL) to lower frequency of 1647  $\text{cm}^{-1}$  (5.00 mg/mL) suggesting more dominant structures forming in octanol as peptide concentration increases.

**Table 2.** The spectral structure components present in GS at 5.00 mg/mL solution, identified in Figure 8. The identified structures are labelled

according to the contributing groups and their response (increase or decrease) to increasing temperature. Values for melting temperature  $\pm$  standard deviation are given.

Wavenumber $\pm 1 \text{ cm}^{-1}$	Group	Signal Response	$T_m$ ( $^{\circ}\text{C}$ ) $\pm 2$
1617	Phe ring	Increase	44
1642	$\beta$ -sheet C=O	Increase $>40$ $^{\circ}\text{C}$	55
1642	$\beta$ -sheet C=O	Decrease $<40$ $^{\circ}\text{C}$	40
1645	Orn $\text{NH}_3^+$	Increase	46
1647	Orn $\text{NH}_3^+$	Increase	43
1650	$\beta$ -sheet C=O	Decrease	45
1685	$\beta$ -turn C=O	Increase	44
1696	$\beta$ -sheet C=O	Increase	47
1699	$\beta$ -sheet C=O	Increase	42

Higher order structures are also present evidenced from the blue-shifted shoulder as depicted Figure S-13. Comparing the concentration and temperature induced structural changes in 2D-IR spectra, with increase in concentration there is loss of diagonal and off-diagonal structures, indicated by blue and black arrow in Figure 10a. The fine structure present at low GS concentrations observed in FTIR, is lost as aggregates form with increasing concentration, as further indicated in Figure S-13 from 2D-IR by loss of the off-diagonal structure related to intermolecular  $\beta$ -sheet-like structures and turns at high frequency. Comparing a 1.00 and 5.00 mg/mL spectra showed that the main absorption band shifted with increasing concentration, which could be an indication of the interactions of a H-bonded network, strengthening the aggregated structures centred near  $1640/5 \text{ cm}^{-1}$  in Figure 10a, Figure S-13. Heating the aggregated structures at 5.00 mg/mL disrupted the aggregates, and they disassemble to reveal/unmask the fine structural details of less aggregated forms and GS monomers presented in Figure 10b. These fine structural details are also observed in octanol at low GS concentration. Therefore, with increasing concentration, the amide I signal is lost as the fine structures of GS are masked within a network of GS aggregates. While with increasing temperature, the interpeptide hydrogen bonds and other weak non-covalent interactions are lost revealing the fine structural details of small GS oligomers and monomers. As previously discussed, this is evidenced by an increase in anharmonicity at high temperature showing reduced coupling, as further shown by the transition dipole analysis.

The thermal event centred at  $T_{m2} = 59 \pm 2$   $^{\circ}\text{C}$  for GS is analogous to the transition temperatures observed in melting of protein structures.<sup>63-70</sup> Depending on the solvent system, it has been observed for proteins that the  $T_m$  of  $\beta$ -sheet structures varies from 60 - 70  $^{\circ}\text{C}$ .<sup>71-73</sup> In an FTIR temperature dependent study by Lewis *et al.*,<sup>74</sup> the GS amide I band of the phospholipid membrane-bound GS was invariant for low temperature range of 20 - 48  $^{\circ}\text{C}$ , however, upon thermal increase and for temperatures above 52  $^{\circ}\text{C}$  there was identified a shift in the amide I band of GS to high wavenumbers which corresponded to shifts in carbonyl and methylene stretches of the lipid matrix.<sup>74</sup>

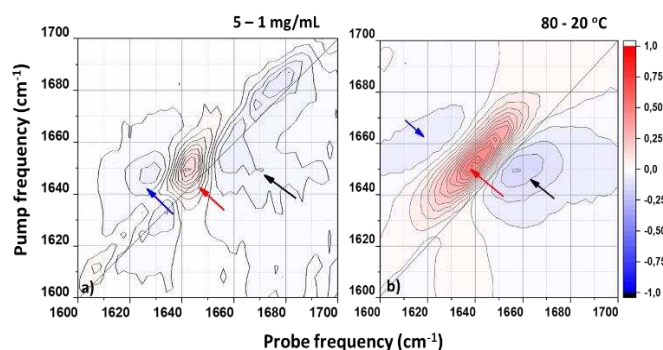
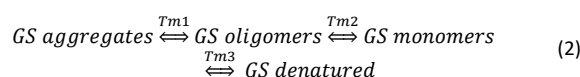


**Figure 10.** Comparison features of (a) GS difference spectra for concentrations 5.00 - 1.00 mg/mL and (b) difference spectrum for temperatures 80 - 20  $^{\circ}\text{C}$  at 5.00 mg/mL.

The conformation of the GS molecule (monomer) has been proposed to remain unchanged under varying conditions, such as high temperatures, solvent variations with different polarity, in micelles, phospholipid bilayers or detergents and even when agents which alter conformation are present.<sup>11,20,69,75</sup> No significant conformation change of the GS monomer was exhibited in the considered temperature range of 20 - 80  $^{\circ}\text{C}$ . In our study, the full denaturation involving breaking of intramolecular H-bonds was not accomplished considering the selected temperature range. In the rigid GS backbone structure, the peptide bonds are buried and involved in intramolecular H-bonds, giving a conformation corresponding to a two-fold  $\beta$ -hairpin with  $\beta$ -sheet configuration.<sup>76</sup> However, at increase of temperatures above  $T_{m2}$ , 2D-IR spectral features revealed an intense elongated feature indicated as a red arrow Figure 10b. This could indicate the loss of some of the intrapeptide H-bonds, but to obtain a fully denatured GS without any intra-peptide H-bond a  $T_m$  higher than 80  $^{\circ}\text{C}$  is expected. Therefore, we apply schema 2 below to show changes in oligomeric state which influence the changes in coupling which are temperature dependent;



where values for  $T_{m1}$  between 41 - 47  $^{\circ}\text{C}$ ,  $T_{m2}$   $59 \pm 2$   $^{\circ}\text{C}$  were determined in this study. Our study correlated with other IR studies on GS. A thermally induced solvent study on GS and its derivatives reported that the peptide molecules gain kinetic energy and overcome hydrophobic interactions within their aggregates.<sup>77</sup> Spectral features from  $\alpha$ - or  $3_{10}$  helices in the region  $1650\text{-}1660 \text{ cm}^{-1}$  for GS at native and at high temperature are absent, as expected for cyclic GS. The presence of  $\beta$ -sheet structures were clearly defined by both 1D and 2D-IR spectroscopy,<sup>78,79</sup> correlating well with our observed results for GS in 1-octanol.

## 5. CONCLUSIONS

Different data analysis methods of our FTIR and 2D-IR analyses of GS in 1-octanol have produced corroborating results between 1D and 2D IR techniques, showing that increasing temperature leads to spectral changes stemming from GS aggregation / oligomerisation. 2D-IR

enabled analysis of the complex aggregated/oligomerised structures of GS in solution due to the better structural resolution it provides and its sensitivity to coupling. The solvent 1-octanol served as a good mimic for membranes, emulating the lipid environment. The results showed the influence of peptide concentration on conformational behaviour; that increasing concentration does not affect the antiparallel  $\beta$ -sheets buried inside the GS monomer structure and that aggregates start forming from low concentrations. At high concentrations, the self-assembly of GS aggregates is driven by the hydrophobic effect and at a temperature of  $T_{m2} = 57 \pm 2$  °C the temperature induced melting of the aggregates/oligomers results in a rapid and significant change of the GS conformation. Two melting scenarios are identified; at  $T_{m1}$  disassembly of oligomers/aggregates reliant on aromatic stacking, interactions with Orn side chain and h-bonds occur, whilst at  $T_{m2}$  there is significant loss of inter-peptide  $\beta$ -sheet-type H-bonds. QM/MM simulations and 2<sup>nd</sup> derivative results revealed additional interactions in which the amino acid side chains of GS partake. Intra- and inter-molecular coupling has a major effect on vibrations of the monomeric GS antiparallel  $\beta$ -strands and  $\beta$ -turns and these are revealed elevated temperatures. This 1D and 2D infrared study contributes to the understanding of GS and its aggregation/oligomerisation state in a membrane-mimicking solvent. Whilst the temperature values for aggregated transitions obtained in 1-octanol are higher than GS would encounter in its natural functional environment, the results demonstrate the ability of FTIR and 2D-IR to accurately differentiate between the different forms of GS. This is the most important characteristic in the GS membrane activity. In order to improve GS activity and selectivity the modulation of the GS oligomerisation by formulation or structure modification must be considered in future studies.

## 6. Associated Content

### Supporting Information

Comparison of normalisation methods for 1D and 2D spectra; normalisation using peak maxima and normalisation at constant frequency (section S1). Docking and simulation of the trimmer model (section S2). Principal Component Analysis (PCA) of FTIR absorption spectra PC1 and PC2 (section S3). Gaussian Peak fitting to FTIR absorption spectra (section S4). 2D-IR spectra and 2D-IR difference spectra for the selected temperature range (section S5). Gaussian peak fittings to 2D-IR slices at 20 and 80 °C with varying anharmonicities (section S6). 2<sup>nd</sup> derivative spectral analysis of IR absorption band at 1 and 5 mg/mL (section S7). Area under 2D-IR diagonal curves plot (section S8). QM/MM spectra for GS monomer model and band assignment (section S9). Concentration effects on structure of GS (section S10). Concentration effects of the structure of GS (section 11).

## 7. AUTHOR INFORMATION

### Corresponding Author

**Pieter H. Neethling** – Department of Physics, Laser Research Institute, Stellenbosch University, Private Bag X1, Matieland 7602, South Africa; Email: [pietern@sun.ac.za](mailto:pietern@sun.ac.za)

## Authors

**Ngaatendwe B. C. Pfukwa** – Department of Physics, Laser Research Institute, Stellenbosch University, Private Bag X1, Matieland 7602, South Africa;

**Marina Rautenbach** - BIOPEP Peptide Group, Department of Biochemistry, Stellenbosch University, Private Bag X1, Matieland 7602, South Africa.

**Neil T. Hunt** - Department of Chemistry and York Biomedical Research Institute, University of York, Heslington, York YO10 5DD, UK

**Olufemi O. Olaoye** - Department of Physics, Laser Research Institute, Stellenbosch University, Private Bag X1, Matieland 7602, South Africa.

**Vikas Kumar** - BIOPEP Peptide Group, Department of Biochemistry, Stellenbosch University, Private Bag X1, Matieland 7602, South Africa.

**Anthony W. Parker** - STFC Central Laser Facility, Research Complex at Harwell, Rutherford Appleton Laboratory, Harwell Science and Innovation Campus, Didcot, Oxon OX11 0QX, United Kingdom

**Lucy Minnes** - Department of Physics, University of Strathclyde, SUPA, 107 Rottenrow East, Glasgow, G4 0NG, United Kingdom.

## Notes

There are no conflicts to declare.

## 8. ACKNOWLEDGEMENTS

We gratefully acknowledge GCRF, Newton Funding project for financial support funding for CP Access and support to the UK Science and Technology Facility Council, Rutherford Appleton Laboratory National facilities were provided through The Global Challenges Research Fund (GCRF), and Newton Funding project. Equipment support and funding was received from the CSIR National Laser Centre Rental Pool Program and student support was received from the African Laser Centre and the South African Research Chair Initiative. The Centre for High Performance Computing in Capetown is also acknowledged.

## 9. REFERENCES

- (1) Eyéghé-Bickong, H. A. Role of Surfactin from *Bacillus Subtilis* in Protection against Antimicrobial Peptides Produced by *Bacillus* Species, University of Stellenbosch, 2011.
- (2) Hackl, E. V.; Berest, V. P.; Gatash, S. V. Interaction of Polypeptide Antibiotic Gramicidin S with Platelets. *Journal of Peptide Science* **2012**, *18* (12), 748–754.
- (3) Ashrafuzzaman, M.; Andersen, O. S.; McElhaney, R. N. The Antimicrobial Peptide Gramicidin S Permeabilizes Phospholipid Bilayer Membranes without Forming Discrete Ion Channels. *Biochim Biophys Acta Biomembr* **2008**, *1778* (12), 2814–2822.
- (4) Ashrafuzzaman, M. The Antimicrobial Peptide Gramicidin s Enhances Membrane Adsorption and Ion Pore Formation

- Potency of Chemotherapy Drugs in Lipid Bilayers. *Membranes (Basel)* **2021**, *11* (247), 1–17.
- (5) Abraham, T.; Prenner, E. J.; Lewis, R. N. A. H.; Mant, C. T.; Keller, S.; Hodges, R. S.; McElhaney, R. N. Structure-Activity Relationships of the Antimicrobial Peptide Gramicidin S and Its Analogs: Aqueous Solubility, Self-Association, Conformation, Antimicrobial Activity and Interaction with Model Lipid Membranes. *Biochim Biophys Acta Biomembr* **2014**, *1838* (5), 1420–1429.
- (6) Staudegger, E.; Prenner, E. J.; Kriechbaum, M.; Degovics, G.; Lewis, R. N. A. H.; McElhaney, R. N.; Lohner, K. X-Ray Studies on the Interaction of the Antimicrobial Peptide Gramicidin S with Microbial Lipid Extracts: Evidence for Cubic Phase Formation. *Biochim Biophys Acta Biomembr* **2000**, *1468* (1–2), 213–230.
- (7) Prenner, E. J.; Lewis, R. N. A. H.; Neuman, K. C.; Gruner, S. M.; Kondejewski, L. H.; Hodges, R. S.; McElhaney, R. N. Nonlamellar Phases Induced by the Interaction of Gramicidin S with Lipid Bilayers. A Possible Relationship to Membrane-Disrupting Activity. *Biochemistry* **1997**, *36* (25), 7906–7916.
- (8) Wenzel, M.; Rautenbach, M.; Vosloo, J. A.; Siersma, T.; Aisenbrey, C. H. M.; Zaitseva, E.; Laubscher, W. E.; van Rensburg, W.; Behrends, J. C.; Bechinger, B.; Hamoen, L. W. The Multifaceted Antibacterial Mechanisms of the Pioneering Peptide Antibiotics Tyrocidine and Gramicidin S. *mBio* **2018**, *9* (5), 1–20.
- (9) Kondejewski, L. H.; Farmer, S. W.; Wishart, D. S.; Kay, C. M.; Hancock, R. E. W.; Hodges, R. S. Modulation of Structure and Antibacterial and Hemolytic Activity by Ring Size in Cyclic Gramicidin S Analogs. *Journal of Biological Chemistry* **1996**, *271* (41), 25261–25268.
- (10) Guan, Q.; Huang, S.; Jin, Y.; Campagne, R.; Alezra, V.; Wan, Y. Recent Advances in the Exploration of Therapeutic Analogues of Gramicidin S, an Old but Still Potent Antimicrobial Peptide. *Journal of Medicinal Chemistry*. 2019, pp 7603–7617.
- (11) Prenner, E. J.; Lewis, R. N. A. H.; McElhaney, R. N. The Interaction of the Antimicrobial Peptide Gramicidin S with Lipid Bilayer Model and Biological Membranes. *Biochimica et Biophysica Acta (BBA) - Biomembranes* **1999**, *1462* (1–2), 201–221.
- (12) Gall, Y. M.; Konashev, M. B. The Discovery of Gramicidin S: The Intellectual Transformation of G.F. Gause from Biologist to Researcher of Antibiotics and on Its Meaning for the Fate of Russian Genetics. *Hist Philos Life Sci* **2001**, *23* (1), 137–150.
- (13) Legrand, B.; Mathieu, L.; Lebrun, A.; Andriamanarivo, S.; Lisowski, V.; Masurier, N.; Zirah, S.; Kang, Y. K.; Martinez, J.; Maillard, L. T. Thiazole-Based  $\gamma$ -Building Blocks as Reverse-Turn Mimetic to Design a Gramicidin S Analogue: Conformational and Biological Evaluation. *Chemistry - A European Journal* **2014**, *20* (22), 6713–6720.
- (14) Hansch, C.; Maloney, P. P.; Fujita, T.; Muir, M. R. Correlation of Biology Activity of Phenoxyacetic Acids with Hammett Substituent Constants and Partition Coefficients. *Nature* **1962**, *194* (4824), 178–180.
- (15) Tetko, I. v.; Livingstone, D. J. Rule-Based Systems to Predict Lipophilicity. In *Comprehensive Medicinal Chemistry II*; Elsevier, 2007; Vol. 5, pp 649–668.
- (16) du Plessis, J.; Pugh, W. J.; Judefeind, A.; Hadgraft, J. Physico-Chemical Determinants of Dermal Drug Delivery: Effects of the Number and Substitution Pattern of Polar Groups. *European Journal of Pharmaceutical Sciences* **2002**, *16* (200), 107–112.
- (17) Du, J.; Pugh, W. J.; Judefeind, A.; Hadgraft, J. The Effect of the Nature of H-Bonding Groups on Diffusion through PDMS Membranes Saturated with Octanol and Toluene. *European Journal of Pharmaceutical Sciences* **2002**, *15*, 63–69.
- (18) Tariq, M. U.; Haseeb, M.; Aledhari, M.; Razzak, R.; Parizi, R. M.; Saeed, F. Methods for Proteogenomics Data Analysis, Challenges, and Scalability Bottlenecks: A Survey. **2016**, *4*, 1–20.
- (19) Engelmann, F. M.; Rocha, S. V. O.; Toma, H. E.; Araki, K.; Baptista, M. S. Determination of N-Octanol/Water Partition and Membrane Binding of Cationic Porphyrins. *Int J Pharm* **2007**, *329*, 12–18.
- (20) Helle, S. S.; Zandstra, P. W. Unusual Surface Tension Behavior of an Aqueous Solution of Gramicidin S. *J Colloid Interface Sci* **1992**, *151* (1), 130–135.
- (21) Llamas-Saiz, A. L.; Grotenbreg, G. M.; Overhand, M.; Van Raaij, M. J. Double-Stranded Helical Twisted  $\beta$ -Sheet Channels in Crystals of Gramicidin S Grown in the Presence of Trifluoroacetic and Hydrochloric Acids. *Acta Crystallogr D Biol Crystallogr* **2007**, *63* (3), 401–407.
- (22) Hume, S.; Greetham, G. M.; Donaldson, P. M.; Towrie, M.; Parker, A. W.; Baker, M. J.; Hunt, N. T. 2D-Infrared Spectroscopy of Proteins in Water: Using the Solvent Thermal Response as an Internal Standard. *Anal Chem* **2020**, *92* (4), 3463–3469.
- (23) Donaldson, P. M.; Greetham, G. M.; Shaw, D. J.; Parker, A. W.; Towrie, M. A 100 KHz Pulse Shaping 2D-IR Spectrometer

- Based on Dual Yb:KGW Amplifiers. *Journal of Physical Chemistry A* **2018**, *122* (3), 780–787.
- (24) Hamm, P.; Lim, M.; Hochstrasser, R. M. Structure of the Amide I Band of Peptides Measured by Femtosecond Nonlinear-Infrared Spectroscopy. *Journal of Physical Chemistry B* **1998**, *102* (31), 6123–6138.
- (25) Hamm, P.; Zanni, M. T. *Concepts and Methods of 2D Infrared Spectroscopy*; Cambridge University Press: New York, 2011.
- (26) Hamm, P.; Helbing, J.; Bredenbeck, J. Two-Dimensional Infrared Spectroscopy of Photoswitchable Peptides. *Physical Chemistry* **2008**, *59*, 291–317.
- (27) Stucki-Buchli, B.; Johnson, P. J. M.; Bozovic, O.; Zanobini, C.; Koziol, K. L.; Hamm, P.; Gulzar, A.; Wolf, S.; Buchenberg, S.; Stock, G. 2D-IR Spectroscopy of an AHA Labeled Photoswitchable PDZ2 Domain. *Journal of Physical Chemistry A* **2017**, *121*, 49, 9435–9445.
- (28) Andresen, E. R.; Hamm, P. Site-Specific Difference 2D-IR Spectroscopy of Bacteriorhodopsin. *Journal of Physical Chemistry B* **2009**, *113* (18), 6520–6527.
- (29) Ramakers, L. A. I.; Hithell, G.; May, J. J.; Greetham, G. M.; Donaldson, P. M.; Towrie, M.; Parker, A. W.; Burley, G. A.; Hunt, N. T. 2D-IR Spectroscopy Shows That Optimised DNA Minor Groove Binding of Hoechst33258 Follows an Induced Fit Model. *J. Phys. Chem. B* **2017**, *121* (1295).
- (30) Deniz, E.; Löffler, J. G.; Kondratiev, A.; Thun, A. R.; Shen, Y.; Wille, G.; Bredenbeck, J. High-Precision Background Correction and Artifact Suppression for Ultrafast Spectroscopy by Quasi-Simultaneous Measurements in a Split-Sample Cell. *Rev. Sci. Instrum* **2022**, *93* (033001), 1–6.
- (31) Shaw, D. J.; Hill, R. E.; Simpson, N.; Hussein, F. S.; Robb, K.; Greetham, G. M.; Towrie, M.; Parker, A. W.; Robinson, D.; Hirst, J. D.; Hoskisson, P. A.; Hunt, N. T. Examining the Role of Protein Structural Dynamics in Drug Resistance in Mycobacterium Tuberculosis. *Chem. Sci* **2017**, *8*, 8384–8399.
- (32) Hume, S.; Hithell, G.; Greetham, G. M.; Donaldson, P. M.; Towrie, M.; Parker, A. W.; Baker, M. J.; Hunt, N. T. Measuring Proteins in H<sub>2</sub>O with 2D-IR Spectroscopy. *Chem. Sci* **2019**, *10*, 6448–6456.
- (33) Minnes, L.; Shaw, D. J.; Cossins, B. P.; Donaldson, P. M.; Greetham, G. M.; Towrie, M.; Parker, A. W.; Baker, M. J.; Henry, A. J.; Taylor, R. J.; Hunt, N. T. Quantifying Secondary Structure Changes in Calmodulin Using 2D-IR Spectroscopy. *Anal Chem* **2017**, *89* (20), 10898–10906.
- (34) Wenzel, M.; Rautenbach, M.; Vosloo, J. A.; Siersma, T.; Aisenbrey, C. H. M.; Zaitseva, E.; Laubscher, W. E.; van Rensburg, W.; Behrends, J. C.; Bechinger, B.; Hamoen, L. W. The Multifaceted Antibacterial Mechanisms of the Pioneering Peptide Antibiotics Tyrocidine and Gramicidin S. *mBio* **2018**, *9* (5), 1–20.
- (35) Rautenbach, M.; Kumar, V.; Vosloo, J. A.; Masoudi, Y.; van Wyk, R. J.; Stander, M. A. Oligomerisation of Tryptocidine C, a Trp-Rich Cyclodecapeptide from the Antimicrobial Tyrothricin Complex. *Biochimie* **2021**, *181*, 123–133.
- (36) Demirdöven, N.; Cheatum, C. M.; Chung, H. S.; Khalil, M.; Knoester, J.; Tokmakoff, A. Two-Dimensional Infrared Spectroscopy of Antiparallel  $\beta$ -Sheet Secondary Structure. *J Am Chem Soc* **2004**, *126* (25), 7981–7990.
- (37) Strasfeld, D. B.; Ling, Y. L.; Gupta, R.; Raleigh, D. P.; Zanni, M. T. Strategies for Extracting Structural Information from 2D IR Spectroscopy of Amyloid: Application to Islet Amyloid Polypeptide. *Journal of Physical Chemistry B* **2009**, *113* (47), 15679–15691.
- (38) Ganim, Z.; Jones, K. C.; Tokmakoff, A. Insulin Dimer Dissociation and Unfolding Revealed by Amide I Two-Dimensional Infrared Spectroscopy. *Physical Chemistry Chemical Physics* **2010**, *12* (14), 3579–3588.
- (39) Kupser, P.; Pagel, K.; Oomens, J.; Polfer, N.; Koks, B.; Meijer, G.; von Helden, G. Amide-I and-II Vibrations of the Cyclic-Sheet Model Peptide Gramicidin S in the Gas Phase. *J. AM. CHEM. SOC* **2010**, *132* (6), 2085–2093.
- (40) Nagornova, N. S.; Rizzo, T. R.; Boyarkin, O. v. Highly Resolved Spectra of Gas-Phase Gramicidin S: A Benchmark for Peptide Structure Calculations. **2010**, *132*, 34.
- (41) Naik, V. M.; Krimm, S.; Denton, J. B.; Nemethy, G.; Scheragai, H. A. Vibrational Analysis of Peptides, Polypeptides and Proteins. *Int J Pept Protein Res* **1984**, *24* (6), 613–626.
- (42) Silva, C. B.; da Silva Filho, J. G.; Pinheiro, G. S.; Teixeira, A. M. R.; Freire, P. T. C. Vibrational and Structural Properties of L-Alanyl-L-Phenylalanine Dipeptide by Raman Spectroscopy, Infrared and DFT Calculations. *Vib Spectrosc* **2018**, *98* (July), 128–133.
- (43) Ji, Y.; Yang, X.; Ji, Z.; Zhu, L.; Ma, N.; Chen, D.; Jia, X.; Tang, J.; Cao, Y. DFT-Calculated IR Spectrum Amide I, II, and III Band Contributions of N-Methylacetamide Fine Components. *ACS Omega* **2020**, *5* (15), 8572–8578.
- (44) Bauschlicher, C. W.; Langhoff, S. R. The Calculation of Accurate Harmonic Frequencies of Large Molecules: The Polycyclic Aromatic Hydrocarbons, a Case Study. *Spectrochim Acta A Mol Biomol Spectrosc* **1997**, *53* (8), 1225–1240.
- (45) Dunkelberger, E. B.; Grechko, M.; Zanni, M. T. Transition Dipoles from 1D and 2D Infrared Spectroscopy Help Reveal the Secondary Structures of Proteins: Application to

- Amyloids. *Journal of Physical Chemistry B* **2015**, *119* (44), 14065–14075.
- (46) Grechko, M.; Zanni, M. T. Quantification of Transition Dipole Strengths Using 1D and 2D Spectroscopy for the Identification of Molecular Structures via Exciton Delocalization: Application to  $\alpha$ -Helices. *Journal of Chemical Physics* **2012**, *137* (18), 184202.
- (47) Hamm, P.; Zanni, M. T. *Concepts and Methods of 2D Infrared Spectroscopy*; Cambridge University Press: New York, 2011.
- (48) Kubelka, J.; Keiderling, T. A. Differentiation of  $\beta$ -Sheet-Forming Structures: Ab Initio-Based Simulations of IR Absorption and Vibrational CD for Model Peptide and Protein  $\beta$ -Sheets. *J Am Chem Soc* **2001**, *123* (48), 12048–12058.
- (49) Davis, C. M.; Zanetti-Polzi, L.; Gruebele, M.; Amadei, A.; Dyer, R. B.; Daidone, I. A Quantitative Connection of Experimental and Simulated Folding Landscapes by Vibrational Spectroscopy. *Chem Sci* **2018**, *9* (48), 9002–9011.
- (50) Cheatum, C. M.; Tokmakoff, A.; Knoester, J. Signatures of  $\beta$ -Sheet Secondary Structures in Linear and Two-Dimensional Infrared Spectroscopy. *Journal of Chemical Physics* **2004**, *120* (17), 8201–8215.
- (51) Bouchard, M.; Zurdo, J.; Nettleton, E. J.; Dobson, C. M.; Robinson, C. V. Formation of Insulin Amyloid Fibrils Followed by FTIR Simultaneously with CD and Electron Microscopy. *Protein Science* **2000**, *9* (10), 1960–1967.
- (52) Shivu, B.; Seshadri, S.; Li, J.; Oberg, K. A.; Uversky, V. N.; Fink, A. L. Distinct  $\beta$ -Sheet Structure in Protein Aggregates Determined by ATR-FTIR Spectroscopy. *Biochemistry* **2013**, *52* (31), 5176–5183.
- (53) Petkov, P.; Lilkova, E.; Ilieva, N.; Litov, L. Self-Association of Antimicrobial Peptides: A Molecular Dynamics Simulation Study on Bombinin. *Int J Mol Sci* **2019**, *20* (5450), 1–14.
- (54) Kuroda, Y.; Suenaga, A.; Sato, Y.; Kosuda, S.; Taiji, M. All-Atom Molecular Dynamics Analysis of Multi-Peptide Systems Reproduces Peptide Solubility in Line with Experimental Observations. *Sci Rep* **2016**, *6* (19479), 1–11.
- (55) Baldwin, R. L. Temperature Dependence of the Hydrophobic Interaction in Protein Folding. *Proc Natl Acad Sci U S A* **1986**, *83* (21), 8069–8072.
- (56) Balasubramanian, D. The Conformation of Gramicidin S in Solution. *J Am Chem Soc* **1967**, *89* (21), 5445–5449.
- (57) Li, J.; Cheng, X.; Lee, J. C. Structure and Dynamics of the Modular Halves of Escherichia Coli Cyclic AMP Receptor Protein. *Biochemistry* **2002**, *41* (50), 14771–14778.
- (58) Barth, A. Infrared Spectroscopy of Proteins. *Biochim Biophys Acta Bioenerg* **2007**, *1767* (9), 1073–1101.
- (59) Piccirilli, F.; Schirò, G.; Vetri, V.; Lupi, S.; Perucchi, A.; Militello, V. Decoding Vibrational States of Concanavalin A Amyloid Fibrils. *Biophys Chem* **2015**, *199*, 17–24.
- (60) Kong, J.; Yu, S. Fourier Transform Infrared Spectroscopic Analysis of Protein Secondary Structures. *Acta Biochim Biophys Sin (Shanghai)* **2007**, *39* (8), 549–559.
- (61) Adochitei, A.; Drochioiu, G. Rapid Characterization of Peptide Secondary Structure by FT-IR Spectroscopy. *Revue Roumaine de Chimie* **2011**, *56* (8), 783–791.
- (62) Miyazawa, M.; Sonoyama, M. Second Derivative near Infrared Studies on the Structural Characterisation of Proteins. *J Near Infrared Spectrosc* **1998**, *6* (1–4), 253–257.
- (63) O'Boyle, F.; Wallace, B. A. The Temperature Dependence of Gramicidin Conformational States in Octanol. *Protein Pept Lett* **2003**, *10* (1), 9–17.
- (64) Arrondo, J. L. R.; Goñi, F. M.; Castresana, J.; Valpuesta, J. M. Structure and Thermal Denaturation of Crystalline and Noncrystalline Cytochrome Oxidase as Studied by Infrared Spectroscopy. *Biochemistry* **1994**, *33* (38), 11650–11655.
- (65) Surewicz, W. K.; Leddy, J. J.; Mantsch, H. H. Structure, Stability, and Receptor Interaction of Cholera Toxin As Studied by Fourier-Transform Infrared Spectroscopy. *Biochemistry* **1990**, *29* (35), 8106–8111.
- (66) Martínez, A.; Haavik, J.; Flatmark, T.; Arrondo, J. L. R.; Muga, A. Conformational Properties and Stability of Tyrosine Hydroxylase Studied by Infrared Spectroscopy. *Journal of Biological Chemistry* **1996**, *271* (33), 19737–19742.
- (67) Chehín, R.; Iloro, I.; Marcos, M. J.; Villar, E.; Shnyrov, V. L.; Arrondo, J. L. R. Thermal and PH-Induced Conformational Changes of a  $\beta$ -Sheet Protein Monitored by Infrared Spectroscopy. *Biochemistry* **1999**, *38* (5), 1525–1530.
- (68) Arrondo, J. L. R.; Blanco, F. J.; Serrano, L.; Goñi, F. M. Infrared Evidence of a  $\beta$ -Hairpin Peptide Structure in Solution. *FEBS Lett* **1996**, *384* (1), 35–37.
- (69) Lewis, R. N. A. H.; Prenner, E. J.; Kondejewski, L. H.; Flach, C. R.; Mendelsohn, R.; Hodges, R. S.; McElhaney, R. N. Fourier Transform Infrared Spectroscopic Studies of the Interaction of the Antimicrobial Peptide Gramicidin S with Lipid Micelles and with Lipid Monolayer and Bilayer Membranes. *Biochemistry* **1999**, *38* (46), 15193–15203.

- (70) Maness, S. J.; Franzen, S.; Gibbs, A. C.; Causgrove, T. P.; Dyer, R. B. Nanosecond Temperature Jump Relaxation Dynamics of Cyclic  $\beta$ -Hairpin Peptides. *Biophys J* **2003**, *84* (6), 3874–3882.
- (71) Brown, L. J.; Singh, L.; Sale, K. L.; Yu, B.; Trent, R.; Fajer, P. G.; Hambly, B. D. Functional and Spectroscopic Studies of a Familial Hypertrophic Cardiomyopathy Mutation in Motif X of Cardiac Myosin Binding Protein-C. *European Biophysics Journal* **2002**, *31* (5), 400–408.
- (72) Wu, J.; Yang, J. T.; Wu, C. S. C.  $\beta$ -II Conformation of All- $\beta$  Proteins Can Be Distinguished from Unordered Form by Circular Dichroism. *Anal Biochem* **1992**, *200* (2), 359–364.
- (73) Markovic-Housley, Z.; Garavito, R. M. Effect of Temperature and Low PH on Structure and Stability of Matrix Porin in Micellar Detergent Solutions. *Biochimica et Biophysica Acta (BBA)/Protein Structure and Molecular* **1986**, *869* (2), 158–170.
- (74) Lewis, R. N. A. H.; Prenner, E. J.; Kondejewski, L. H.; Flach, C. R.; Mendelsohn, R.; Hodges, R. S.; McElhaney, R. N. Fourier Transform Infrared Spectroscopic Studies of the Interaction of the Antimicrobial Peptide Gramicidin S with Lipid Micelles and with Lipid Monolayer and Bilayer Membranes. *Biochemistry* **1999**, *38* (46), 15193–15203.
- (75) Jelokhani-Niaraki, M.; Kondejewski, L. H.; Farmer, S. W.; Hancock, R. E. W.; Kay, C. M.; Hodges, R. S. Diastereoisomeric Analogues of Gramicidin S: Structure, Biological Activity and Interaction with Lipid Bilayers. *Biochemical Journal* **2000**, *349* (3), 747–755.
- (76) Luo, J.; Otero, J. M.; Yu, C. H.; Wärmländer, S. K. T. S.; Gräslund, A.; Overhand, M.; Abrahams, J. P. Inhibiting and Reversing Amyloid- $\beta$  Peptide (1-40) Fibril Formation with Gramicidin S and Engineered Analogues. *Chemistry - A European Journal* **2013**, *19* (51), 17338–17348.
- (77) Jelokhani-Niaraki, M.; Prenner, E. J.; Kay, C. M.; McElhaney, R. N.; Hodges, R. S.; Kondejewski, L. H. Conformation and Other Biophysical Properties of Cyclic Antimicrobial Peptides in Aqueous Solutions. *Journal of Peptide Research* **2001**, *58* (4), 293–306.
- (78) Stevenson, P.; Tokmakoff, A. Distinguishing Gramicidin D Conformers through Two-Dimensional Infrared Spectroscopy of Vibrational Excitons. *Journal of Chemical Physics* **2015**, *142* (21).
- (79) Demirdöven, N.; Cheatum, C. M.; Chung, H. S.; Khalil, M.; Knoester, J.; Tokmakoff, A. Two-Dimensional Infrared Spectroscopy of Antiparallel  $\beta$ -Sheet Secondary Structure. *J Am Chem Soc* **2004**, *126* (25), 7981–7990.

## Table of Contents (TOC) Graphics

